doi:10.1093/plphys/kiab451 PLANT PHYSIOLOGY 2022: 188: 593–607

Plant Physiology®

Research Article

# MiR398-regulated antioxidants contribute to *Bamboo mosaic virus* accumulation and symptom manifestation

**Kuan-Yu Lin** [1], **Su-Yao Wu**[1,†], **Yau-Heiu Hsu** [2] and **Na-Sheng Lin** [1,*,‡]

1 Institute of Plant and Microbial Biology, Academia Sinica, Taipei 11529, Taiwan
2 Graduate Institute of Biotechnology, National Chung Hsing University, Taichung 40227, Taiwan

*Author for communication: nslin@sinica.edu.tw
†Present address: Office of Science and Technology, Executive Yuan, Taipei, Taiwan.
‡Senior author.

*Bamboo mosaic virus* manipulates reactive oxygen species scavengers to enhance replication and symptom formation.

K.-Y. Lin, Y.-H. Hsu, and N.-S. Lin designed the studies and analyzed the data; K.-Y. Lin and S.-Y. Wu performed the experiments; K.-Y. Lin wrote and N.-S. Lin supervised the writing with inputs from all authors.

The author responsible for distribution of materials integral to the findings presented in this article in accordance with the policy described in the Instructions for Authors (https://academic.oup.com/plphys/pages/general-instructions) is: Na-Sheng Lin (nslin@sinica.edu.tw).

## Abstract

Virus infections that cause mosaic or mottling in leaves commonly also induce increased levels of reactive oxygen species (ROS). However, how ROS contributes to symptoms is less well documented. *Bamboo mosaic virus* (BaMV) causes chlorotic mosaic symptoms in both *Brachypodium distachyon and Nicotiana benthamiana*. The BaMV △CPN35 mutant with an N-terminal deletion of its coat protein gene exhibits asymptomatic infection independently of virus titer. Histochemical staining of ROS in mock-, BaMV-, and BaMV△CPN35-infected leaves revealed that hydrogen peroxide ($H_2O_2$) accumulated solely in BaMV-induced chlorotic spots. Moreover, exogenous $H_2O_2$ treatment enhanced yellowish chlorosis in BaMV-infected leaves. Both BaMV and BaMV△CPN35 infection could induce the expression of Cu/Zu superoxide dismutase (CSD) antioxidants at messenger RNA and protein level. However, BaMV triggered the abundant accumulation of full-length NbCSD2 preprotein (prNbCSD2, without transit peptide cleavage), whereas BaMV△CPN35 induced a truncated prNbCSD2. Confocal microscopy showed that majority of NbCSD2-green fluorescent protein (GFP) predominantly localized in the cytosol upon BaMV infection, but BaMV△CPN35 infection tended to cause NbCSD2-GFP to remain in chloroplasts. By 5′-RNA ligase-mediated rapid amplification of cDNA ends, we validated CSDs are the targets of miR398 in vivo. Furthermore, BaMV infection increased the level of miR398, while the level of BaMV titer was regulated positively by miR398 but negatively by CSD2. In contrast, overexpression of cytosolic form NbCSD2, impairing the transport into chloroplasts, greatly enhanced BaMV accumulation. Taken together, our results indicate that induction of miR398 by BaMV infection may facilitate viral titer accumulation, and cytosolic prNbCSD2 induction may contribute to $H_2O_2$ accumulation, resulting in the development of BaMV chlorotic symptoms in plants.

Received February 11, 2021. Accepted August 27, 2021. Advance access publication September 21, 2021



Open Access

## Introduction

Plants have evolved sophisticated mechanisms to sense and respond to unfavorable environmental cues. Production of reactive oxygen species (ROS) is a common plant response to various biotic and abiotic stresses. As a very dynamic signaling compartment, chloroplasts can sense biotic and abiotic perturbations to produce pro-defense molecules, including hormones such as salicylic, jasmonic and abscisic acids (ABAs), as well as secondary messengers (calcium and ROS) (Serrano et al., 2016). Typically, virus infection rapidly increases ROS levels (termed an oxidative burst), including hydroxyl radicals ($^{\cdot}OH$), superoxide anions ($O^{\cdot-2}$) and hydrogen peroxide ($H_2O_2$). SUPEROXIDE DISMUTASES (SODs) are important ROS scavengers in plant cells that convert $O^{\cdot-2}$ to $H_2O_2$ in the first step of the detoxifying process during pathogen-induced oxidative burst (Desikan et al., 1996), but SOD activity is differentially regulated among diverse virus-infected plants (Allan et al., 2001; Clarke et al., 2002). The balance between increased oxidative stress and antioxidant levels mediates symptom development in systemically virus-infected plants (Riedle-Bauer, 2000; Hakmaoui et al., 2012). Photosystems I and II in chloroplasts are the primary ROS-generating centers, which are rich in oxygen, reductants, and high-energy intermediates (Asada, 2006).

Studies have shown that stress-responsive genes are tightly regulated and fine-tuned by a group of small RNAs (sRNAs), termed microRNAs (miRNAs) (Sunkar et al., 2012). Plant miRNAs are a class of endogenous sRNAs of 20–24 nt that modulate biological and developmental events by negatively regulating gene expression via degradation or translational repression of messenger RNAs (mRNAs) (Wang et al., 2019). In *Arabidopsis thaliana*, primary miRNAs with characteristic imperfect stem-loop or hairpin structures are transcribed by RNA polymerase II from *MIR* genes and then catalyzed by DICER-LIKE 1 (DCL1), HYPONASTIC LEAVES 1 (HYL1), DOUBLE-STRANDED RNA-BINDING PROTEIN (DRB) 1/2, and SERRATE (SE) to generate precursor miRNAs (pre-miRNAs). Pre-miRNAs are processed into a 20- to 24-nt miRNA duplex by DCL1, HYL1, and SE, and then methylated at the 3′-terminus by HUA ENHANCER 1, before being exported into the cytoplasm by HASTY 1. In general, miRNA-5p (from the 5′-arm) of the miRNA duplex loads into AGRONAUTE 1 (AGO1) to form an active RNA-induced silencing complex (RISC), which guides RISC to bind target transcripts of complementary sequence. Expression of miRNA target genes is repressed by mRNA cleavage or via a nondegradative mechanism (translational repression) determined by the DCL1 partner proteins, DRB1/2 (Reis et al., 2015).

Virus infection alters the profile of sRNAs by generating virus-derived sRNAs and altering endogenous sRNAs (Zhang et al., 2015), including miRNA accumulation (Mengistu and Tenkegna, 2021). Virus infection can even activate miRNA gene transcription (Bazzini et al., 2009). Constitutive expression of VIRAL SUPPRESSOR OF RNA SILENCING was able to alter miRNA levels and activity (Lewsey et al., 2007; Schott et al., 2012). Apart from miRNAs, a class of virus-activated host-encoded small RNAs (vasiRNAs) may also be induced by RNA virus infection, with some vasiRNAs having been characterized to target genes important in plant immunity (Cao et al., 2014). Studies in animal systems have shown that miRNAs may directly target RNA viruses to restrict (Otsuka et al., 2007; Trobaugh et al., 2014, 2019) or, rather surprisingly, enhance infection (Jopling et al., 2005; Schult et al., 2018). As yet, there is no direct evidence showing direct binding of miRNAs to plant viral genomes, except for some in silico analyses (Satish et al., 2019). However, it has been demonstrated that plant RNA viruses can hijack miRNAs to suppress innate immunity, supporting the notion that viruses manipulate miRNAs to generate a more permissive environment for viral accumulation (He et al., 2008; Varallyay et al., 2010; Li et al., 2012). However, how these virus-responsive miRNAs are regulated has not yet been fully understood.

miR398 is one of the best studied stress-responsive miRNAs and it is evolutionarily well-conserved across the plant kingdom. miR398-3p accumulation is mediated by various abiotic and biotic stresses including salinity, ABA, light, heat, sucrose, copper and iron concentrations, nitrogen deficiency, oxidative stress, and infection by bacteria, fungi, or viruses (Sunkar et al., 2006; Tagami et al., 2007; Dugas and Bartel, 2008; Jagadeeswaran et al., 2009; Jia et al., 2009; Beauclair et al., 2010; Li et al., 2010; Lu et al., 2010; Wu et al., 2011; Liang et al., 2012; Liu et al., 2020). *Arabidopsis thaliana* possesses three miR398-type miRNAs: miR398a (5p-AAGGAGUGGCAUGUGAACACA and 3p-UGUGUUCUCAGGUCACCCCUU), miR398b (5p-AGGGUUGAUAUGAGAACACAC and 3p-UGUGUUCUCAGGUCACCCCUG), and miR398c (5p-AGGGUUGAUAUGAGAACACAC and 3p-UGUGUUCUCAGGUCACCCCUG) (Sunkar and Zhu, 2004). miR398-3p targets cytosolic (CSD1) and chloroplastic (CSD2) forms of the Cu/Zu SOD, COPPER CHAPERONE FOR SUPEROXIDE DISMUTASE (CCS), MITOCHONDRIAL CYTOCHROME OXIDASE SUBUNIT V (COX5), BLUE COPPER-BINDING PROTEIN (BCBP), and an incompletely annotated plastocyanin-like domain-containing protein, of which the expression is altered according to changing miR398 levels (Sunkar et al., 2006; Beauclair et al., 2010; Li et al., 2010; Brousse et al., 2014). miR398b,c regulate CSD2 and CCS via mRNA cleavage and translational repression (Beauclair et al., 2010), but CSD1, COX5, and BCBP expression is regulated by miR398 at the mRNA level (Sunkar et al., 2006; Yamasaki et al., 2007; Brousse et al., 2014). It is also known that miR398b,c is transcribed by the *SQUAMOSA* PROMOTER BINDING PROTEIN-LIKE7 transcription factor under copper-limiting conditions (Sunkar et al., 2006; Dugas and Bartel, 2008; Yamasaki et al., 2009), but CSD2 transcription is unaffected by the presence or absence of copper (Yamasaki et al., 2007). Although multiple studies have shown that miR398 hyper-accumulates in various virus-infected plant species (Tagami et al., 2007; Naqvi et al., 2010; Bazzini et al., 2011; Hu et al., 2011; Pacheco et al., 2012;

Abreu et al., 2014; Suzuki et al., 2019), the biological roles of this group of miRNAs remain unclear. Recently, it was reported that lethal systemic necrosis in potato spindle tuber viroid-infected DCL2/4-knockdown transgenic *Solanum lycopersicum* is accompanied by miR398 upregulation and ROS overproduction (Suzuki et al., 2019). Moreover, increased miR398 accompanied by reduced level of its target umecyanin activates the plant defense responses to restrict beet necrosis yellow vein virus infection in *Nicotiana benthamiana* (Liu et al., 2020).

*Bamboo mosaic virus* (BaMV), a potexvirus of the alphavirus-like superfamily, contains a single-stranded, positive-sense RNA genome with a 5′-$^{7}$mGpppG cap structure and a 3′-poly(A) tail. The viral genome comprises 6,400 nt (excluding the 3′-poly(A) tail), with five conserved open reading frames (ORFs) flanked by 5′- and 3′-untranslated regions (UTRs) of 94 and 142 nt, respectively (Lin et al., 1992, 1994; Yang et al., 1997). ORF 1 encodes a 155-kDa replicase containing three functional domains, i.e. methyltransferase (Li et al., 2001; Huang et al., 2004), helicase (Li et al., 2001), and RdRp (Li et al., 1998) domains. ORFs 2–4 are triple gene block protein (TGBp) genes that encode TGBp1–3 of 28, 13, and 6 kDa, respectively (Lin et al., 1994; Yang et al., 1997) . All three TGBps are required for BaMV cell-to-cell movement (Wung et al., 1999; Lin et al., 2004; Lin et al., 2006). ORF 5 encodes the 25-kDa coat protein (CP), which is expressed by a 1.0-kb subgenomic RNA (Lin et al., 1992). BaMV CP is involved in virus encapsidation, cell-to-cell movement, and also a symptom determinant in BaMV-infected *N. benthamiana* (Lan et al., 2010; Lee et al., 2011; DiMaio et al., 2015). The BaMV△CPN35 mutant, in which the N-terminal 35 amino acids (aa) of the *CP* gene have been deleted, results in asymptomatic infection in *N. benthamiana*, independently of viral titer (Lan et al., 2010). In addition, BaMV can induce symptomless infection in *A. thaliana* but the virus cannot move to non-inoculated leaves (ILs) (Lin et al., 2010).

In this study, we used wild-type (WT) symptomatic BaMV and asymptomatic BaMV△CPN35 mutant to address the possible role of miR398 in virus accumulation and symptom formation. We found that miR398 is a positive regulator for BaMV accumulation but its target NbCSD2 is a negative regulator. Both WT BaMV and BaMV△CPN35 infection could induce NbCSD level. However, only WT BaMV infection triggered unprocessed full-length NbCSD2 resided in the cytoplasm and triggered high level accumulation of $H_2O_2$, thereby resulting in chlorotic symptoms in BaMV-infected *N. benthamiana*.

## Results

### $H_2O_2$ accumulates in BaMV-induced symptomatic tissues

BaMV infection causes yellowish mosaic and chlorotic symptoms in *N. benthamiana*, with the N-terminal 35 aa of BaMV CP being symptom determinant (Lan et al., 2010). In *Brachypodium distachyon*, BaMV induces brown stripes and some light green spots in inoculated and systemic leaves (SLs) (Liou et al., 2014). In contrast, BaMV△CPN35 infection is symptomless in these two plants (Supplemental Figures S1, B and C). Typically, ROS accumulation and enhanced antioxidant levels accompany symptom development in compatible virus–plant interactions (Song et al., 2009; Rodriguez et al., 2012; Huseynova et al., 2014; Shang et al., 2018). Thus, we wondered if BaMV induces symptoms related to the plants' ROS response.

We ILs of *N. benthamiana and B. distachyon* with BaMV and BaMV△CPN35 virions and then harvested them at 10-d post-inoculation (dpi) when BaMV infection had induced mosaic symptoms. *In situ* histochemical staining of superoxide and $H_2O_2$ revealed that superoxide distribution was not associated with BaMV-induced symptoms. Superoxide levels were higher in mock-treated relative to BaMV- or BaMV△CPN35- ILs (Figure 1A). However, $H_2O_2$ only accumulated in symptomatic regions of BaMV- but not BaMV△CPN35-infected IL and SLs of both *N. benthamiana and B. distachyon* (Figure 1, B and C; Supplemental Figure S2). Thus, $H_2O_2$ localized in the yellowish mosaic spots of *N. benthamiana* and in the dark brown stripes of *B. distachyon*. Accordingly, accumulation of $H_2O_2$, but not superoxide, appears to be restricted to BaMV infection-induced symptomatic tissues.

### NbCSD1 and NbCSD2 are induced at RNA and protein levels by both BaMV and BaMV△CPN35 infection

There are two possibilities why $H_2O_2$ accumulates in the chlorotic mosaic spots of BaMV-infected leaves: higher SOD activity or repressed photosynthesis, with this latter resulting in lower superoxide formation during photosynthetic electron transport in BaMV-infected plants compared to that in mock-infected plants. However, superoxide levels in BaMV- and BaMV△CPN35-inoculated *N. benthamiana* leaves were comparable, despite $H_2O_2$ levels being undetectable in BaMV△CPN35-ILs by in situ histochemical staining (Figure 1, A–C). These results imply that the higher $H_2O_2$ level in BaMV- than that in mock- or BaMV△CPN35-infected plants may be due to greater SOD activity. SODs can be classified into three groups: CSDs, iron SOD (FeSOD), and manganese SOD (MnSOD), which are localized in cytosol/chloroplasts, peroxisomes/chloroplasts, and mitochondria/peroxisomes, respectively. Superoxides are removed from chloroplasts by FeSOD and CSD (Pilon et al., 2011). An *in gel* SOD activity assay revealed higher CSD activity in BaMV ILs relative to those in mock and BaMV△CPN35 infection at 10 dpi (Supplemental Figure S3).

To confirm that result, we conducted a BLAST analysis on the AtCSD1 and AtCSD2 sequences against the *N. benthamiana* genome and transcriptome database (http://benthgenome.qut.edu.au/) (Nakasugi et al., 2013) and found that NbCSD1 (Nbv5.1tr6233164) is cytosolic and NbCSD2 (Nbv5.1tr6229677) is chloroplastic. We designed specific primers to clone full-length cDNAs of *NbCSD1 and NbCSD2* by

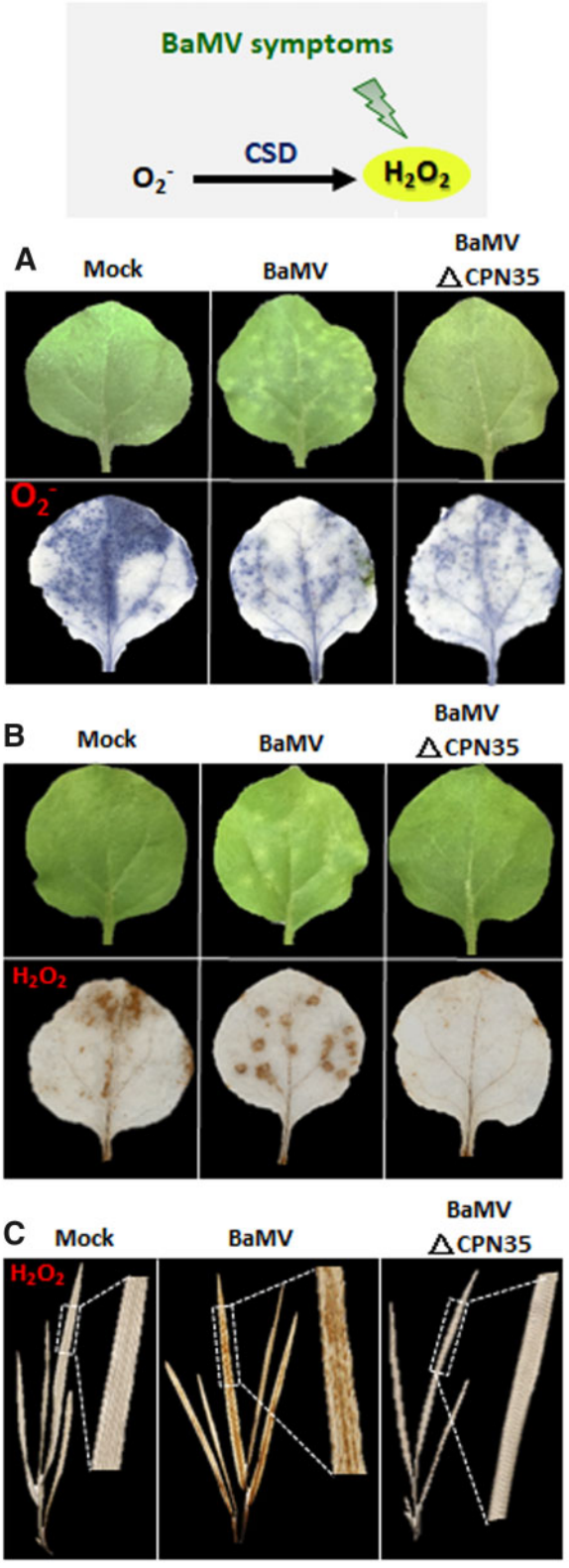


**Figure 1** $H_2O_2$ accumulated in BaMV-induced chlorotic tissues. Histochemical detection of (A) superoxide by Nitrotetrazolium blue chloride and (B and C) $H_2O_2$ accumulation by DAB staining of mock-, BaMV-, and BaMV△CPN35-infected ILs in *N. benthamiana* (B) and *B. distachyon* (C) at 10 dpi. The images were digitally extracted for comparison.

reverse transcription PCR (RT-PCR) and conducted 5′-rapid amplification of cDNA ends (RACE) on WT *N. benthamiana*. We found that the NbCSD1 and AtCSD1 proteins share 70% identity, whereas NbCSD2 and AtCSD2 proteins share 80% identity. Unlike the conserved N-terminal and central regions of NbCSD1 and AtCSD1, the N-terminal transit peptide regions of AtCSD2 and NbCSD2 are hypervariable, yet the SOD motifs of AtCSDs and NbCSDs are highly conserved (Supplemental Figure S4, A–C).

We did not observe any difference in viral CP and TGBp1 levels between BaMV- and BaMV△CPN35-infected leaves by western blot (Figure 2B). However, RNA and protein levels of NbCSD1 and NbCSD2 were increased in BaMV△CPN35-infected leaves, and slightly more so in BaMV-infected leaves, relative to mock-infected leaves (Figure 2, A and B). Notably, NbCSD2 was undetectable in mock-infected plants. However, rather than mature NbCSD2 (i.e. lacking transit peptide, ∼20 kDa), we detected NbCSD2 preprotein (∼31 kDa, prNbCSD2) or a truncated prNbCSD2 (∼28 kDa) using anti-CSD2 in BaMV- or BaMV△CPN35-infected leaves, respectively (Figure 2B). Thus, BaMV and BaMV△CPN35 infection induces expression of NbCSD1 and NbCSD2 in infected *N. benthamiana*.

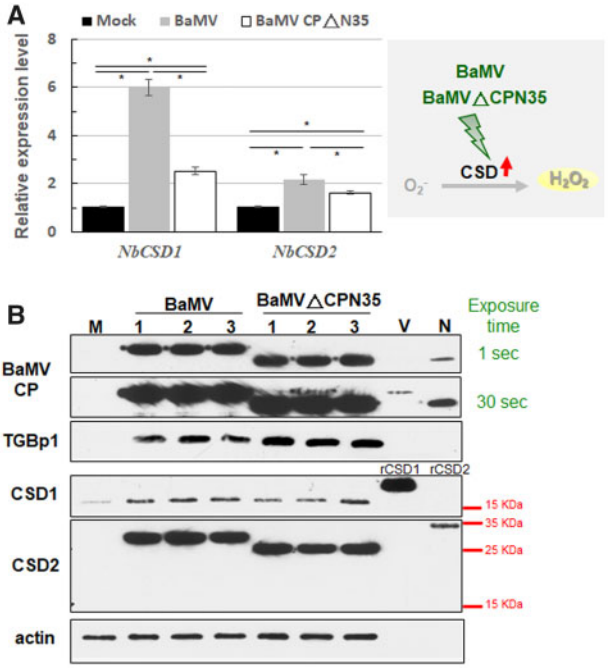


**Figure 2** Differential expression of NbCSD1 and NbCSD2 induced by BaMV and BaMV△CPN35 at RNA and protein level. A, *NbCSD1 and NbCSD2* levels by RT-qPCR and B, BaMV TGBp1 and CP, NbCSD1 and NbCSD2 expression by protein blot in the ILs at 5 dpi in mock-, BaMV-, and BaMV△CPN35-infected *N. benthamiana*. Results from three independent experiments of (A) were used for student's *t* test. $^*P < 0.05$. M: mock inoculation. V: BaMV virion. N: BaMV△CPN35 virion. rCSD1 and rCSD2: recombinant CSD1 and CSD2 protein. Results from three independent experiments, three plants per treatment per experiment, were used for student's *t* test. $^*P < 0.05$.

## NbCSD2 resides in chloroplasts but targets to cytosol upon BaMV infection

BaMV infection induced accumulation of prNbCSD2 rather than mature NbCSD2 (Figure 2B). We hypothesized that this outcome was due to failed targeting of NbCSD2 into chloroplasts. Therefore, we generated a CSD2- green fluorescent protein (GFP) construct and coinfiltrated it with BaMV or BaMV△CPN35 to visualize the subcellular localization of NbCSD2. We used CSD2_noTP-GFP harboring mutations at two positively charged residues within the transit peptide as a control (Figure 3A). As expected, in mock-infiltrated cells, CSD2-GFP localized solely in chloroplasts, whereas CSD2_noTP-GFP resided in both cytosol and chloroplasts (Figure 3, A and B). However, in BaMV-infected cells, CSD2-GFP signal mostly emanated from cytosol at the cell periphery and was limited from chloroplasts. In contrast, in BaMV△CPN35-infected cells, CSD2-GFP signal was mostly associated with chloroplasts and much less so in cytosol (Figure 3B). Thus, we hypothesize that BaMV infection not only induces expression of NbCSD2, but also affects chloroplast targeting of that protein.

## $H_2O_2$ enhances BaMV-induced chlorotic symptoms in *N. benthamiana*

We already showed that $H_2O_2$ accumulated in the chlorotic spots of BaMV-infected *N. benthamiana* leaves but not in symptomless BaMV△CPN35-infected leaves (Figure 1). Accordingly, we tested if $H_2O_2$ affects BaMV-induced symptom development by spraying $H_2O_2$ onto leaves before or after BaMV and BaMV△CPN35 inoculation. As expected, BaMV infection caused chlorotic spots on *N. benthamiana* leaves at 10 dpi. However, the BaMV-infected leaves with $H_2O_2$ treatment either before or after virus inoculation developed more yellowish and bigger chlorotic spots than those without $H_2O_2$ treatment (Figure 4, A and B). However, no symptoms appeared on the BaMV△CPN35-ILs, whether or not they had been treated with $H_2O_2$ (Figure 4A). Moreover, either spraying with $H_2O_2$ pre- or post-inoculation did not alter virus accumulation in the BaMV- and BaMV△CPN35-ILs, as revealed by western blot (Figure 4C). Thus, our results reinforce the notion that $H_2O_2$ could intensify BaMV-induced symptom development without altering BaMV level.

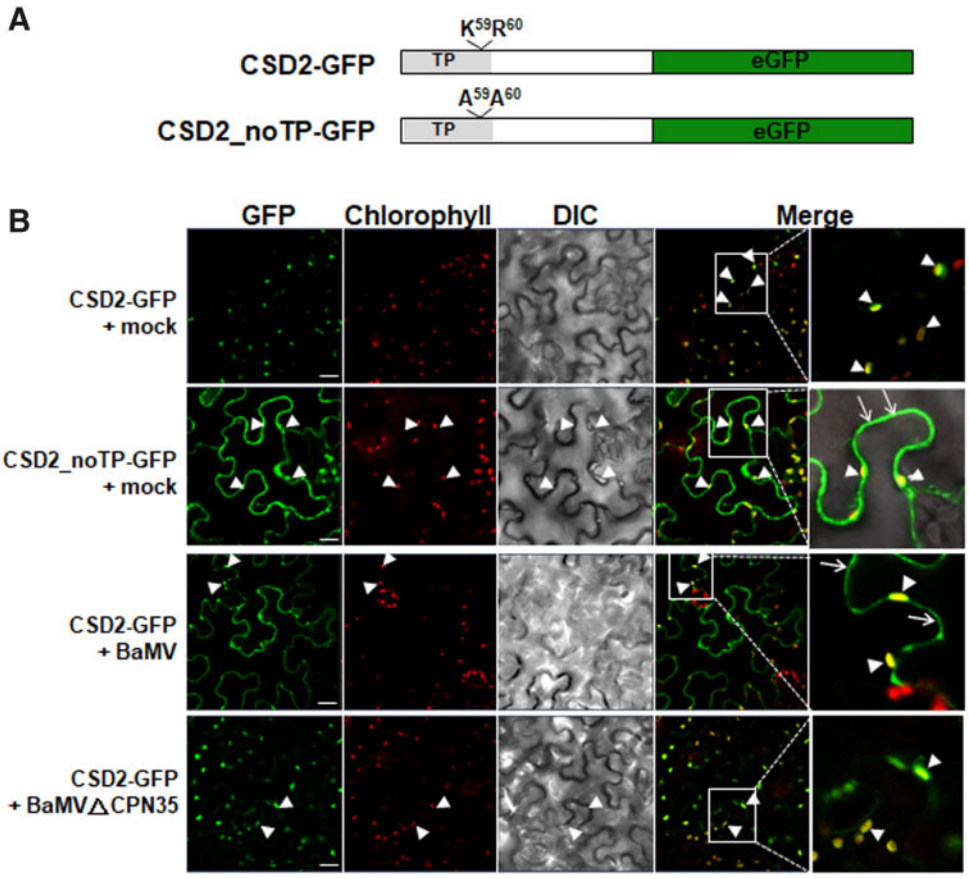


**Figure 3** Subcellular localization of CSD2 and CSD2_noTP fusion with GFP (CSD2-GFP and CSD2_noTP-GFP) in mock-, BaMV-, and BaMV△CPN35-infected *N. benthamiana*. A, Schematic diagram of CSD2-GFP and CSD2_noTP-GFP. Gray box indicates transit peptide (TP). B, Fluorescent signals of CSD2-GFP and CSD2_noTP-GFP in mock-, BaMV-, and BaMV △CPN35-infected leaves by confocal microscopic observation. Scale bar indicates 20 μm. Arrowheads indicate localization of GFP signals in chloroplasts. Arrows indicate localization of GFP signals in cytosol. The images of (B) last column were digitally extracted and enlarged for comparison.

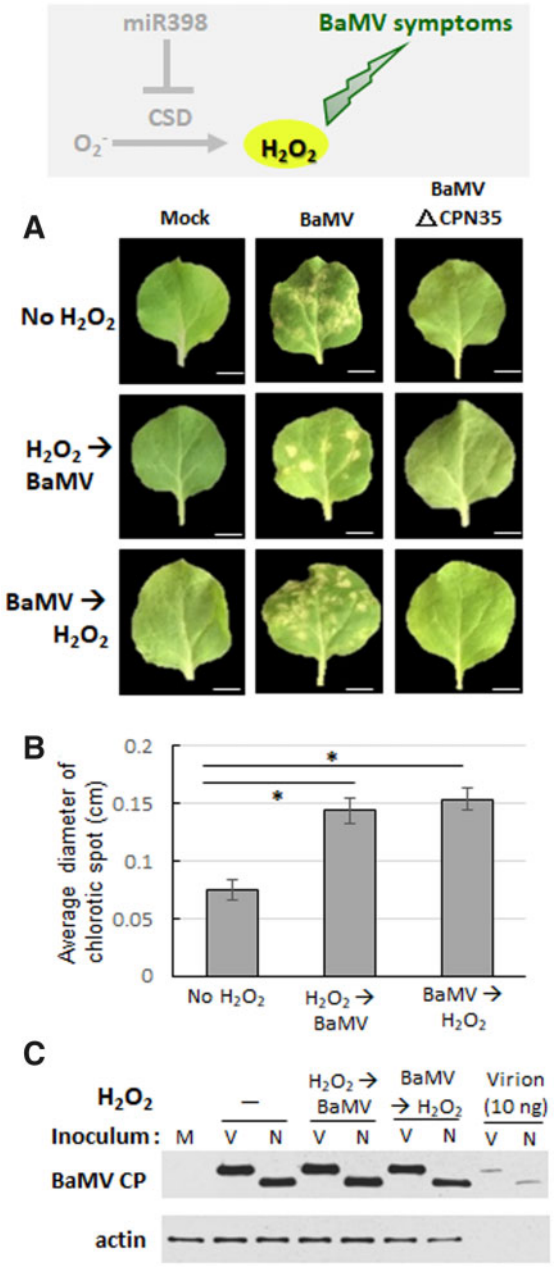


**Figure 4** $H_2O_2$ enhanced BaMV-induced chlorotic symptoms. A, Symptoms and B, quantification of chlorotic spot diameters and C, BaMV CP level by protein blot of mock- (M), BaMV- (V) and BaMV△CPN35 (N)- ILs in *N. benthamiana* at 10 dpi. $H_2O_2$ was sprayed before ($H_2O_2$ → BaMV) or after (BaMV → $H_2O_2$) inoculation at 4-h interval. Scale bar indicates 0.5 cm. Results from five spots of every ILs of three plants from each treatment per experiment were used for student's *t* test by three independent experiments. *$P < 0.05$.

## *NbCSD1* and *NbCSD2* are targets of Nb-miR398

CSDs are regulated by a conserved miRNA in plants, miR398, as revealed by 5′-RNA ligase-mediated RACEs (RLM-RACE) of Arabidopsis (Sunkar and Zhu, 2004), by in vivo assay in *Oryza sativa* (Lu, 2010), and in silico prediction in *Pinus* (Dugas and Bartel, 2008). Sequence alignment also revealed that a miR398-complementary site exists within the 5′-UTR of NbCSD1 and the coding region of NbCSD2. Therefore, we adapted 5′-RLM-RACE to confirm the presence of Nb-miR398 sites in *NbCSD1 and NbCSD2*.

Arabidopsis miR398 precursor (pre-miR398) and cDNAs of *NbCSD1* or *NbCSD2* were cloned into pBin vector for transient overexpression. Leaves of *N. benthamiana* were then co-infiltrated with *Agrobacterium tumefaciens* harboring pBin-miR398 and pBin-NbCSD1-cDNA or pBin-NbCSD2-cDNA, before being harvested for RNA purification at 5-d post-agroinfiltration (dpa). By 5′-RLM-RACE PCR followed by sequencing, miR398b-3p cleaved *NbCSD1* within the 5′-UTR, whereas it cleaved the NbCSD2 ORF between the 10th and 11th nt of the miR398b-3p complementary site (Figure 5A). Furthermore, we used the *Cabbage leaf curl virus* (*CaLCuV*) vector, pCVA-miR398, to transiently overexpress Arabidopsis miR398 precursor in *N. benthamiana*, enabling us to analyze miR398-mediated regulation of *NbCSD1 and NbCSD2* in vivo. In miR398-overexpressing leaves, miR398b level increased 11.4-fold relative to that in vector-control-infiltrated leaves at 5 dpa, whereas NbCSD1 and NbCSD2 levels diminished ∼0.65-fold compared to vector control (Figure 5, B and C). Thus, miR398 indeed downregulates *NbCSD1 and NbCSD2* expression in *N. benthamiana* in vivo via transcript cleavage.

## miR398 is induced upon BaMV infection in *N. benthamiana*

It has been reported previously that levels of miR398-3p change under both biotic and abiotic stresses in Arabidopsis (ZHu et al., 2011), and that expression of miR398-3p and its target genes, *CSD1 and CSD2*, is important for oxidative stress tolerance (Sunkar et al., 2006). Consequently, to determine if BaMV and BaMV△CPN35 infection induce accumulation of NbmiR398b-3p, we inoculated *N. benthamiana* with BaMV or BaMV△CPN35 virions and harvested the ILs at 5 and 10 dpi. Northern blot showed higher levels of NbmiR398-3p in both BaMV- and BaMV△CPN35-ILs at 10 dpi relative to the mock ILs of WT plants at 10 dpi (Figure 6A). Moreover, levels of NbmiR398-3p were higher in the BaMV ILs than BaMV△CPN35 ILs (Figure 6A). To monitor how NbmiR398-3p levels were affected by BaMV infection, we analyzed NbmiR398-3p expression in mock- and BaMV ILs at 2-d intervals from 1 to 9 dpi by means of stem-loop RT-qPCR. Our results show that levels of NbmiR398-3p increased progressively with infection duration in both mock- and BaMV ILs. Notably, BaMV infection induced significantly higher NbmiR398-3p levels at 7 dpi, i.e. when mosaic symptoms appear in *N. benthamiana* (Figure 6B). Thus, mechanical inoculation of BaMV induced NbmiR398-3p upregulation, which coincided with the timepoint when disease symptoms are observed in *N. benthamiana*.

## BaMV levels are regulated positively by miR398 and negatively by CSD2

To further investigate the effects of NbmiR398b-3p on BaMV accumulation, we coinfiltrated *N. benthamiana* with

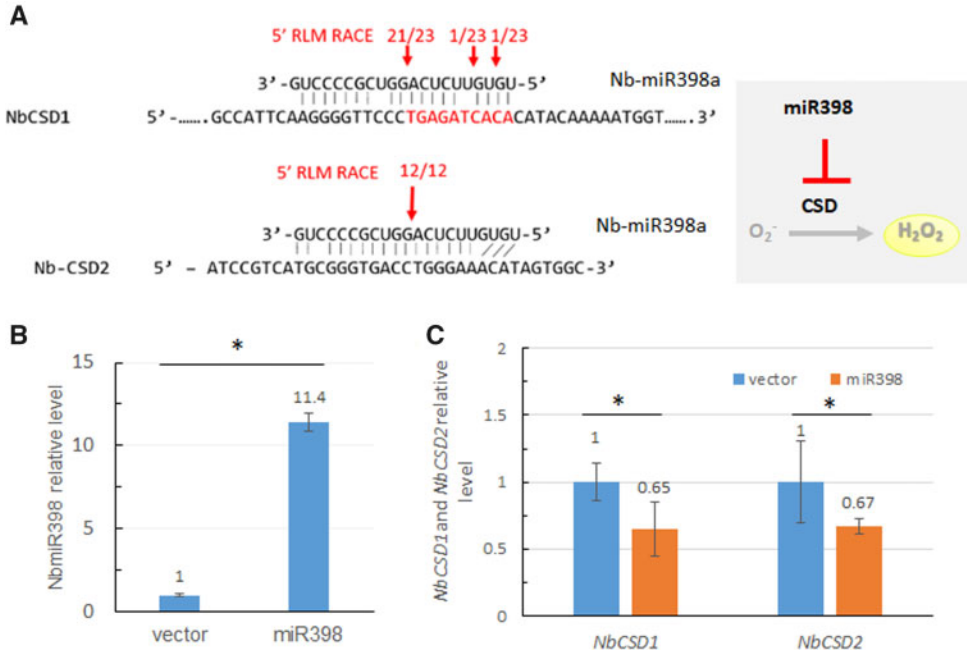


**Figure 5** NbCSD1 and NbCSD2 were the targets of Nb-miR398. Nb-miR398 targets NbCSD1 and NbCSD2 by (A) 5′-RLM-RACE and in vivo assay of transiently overexpressed miR398 in *N. benthamiana*. B, miR398 and C, *NbCSD1 and NbCSD2* levels were quantified by RT-qPCR. Results from three independent experiments, three plants per treatment per experiment, were used for student's *t* test. *$P < 0.05$.

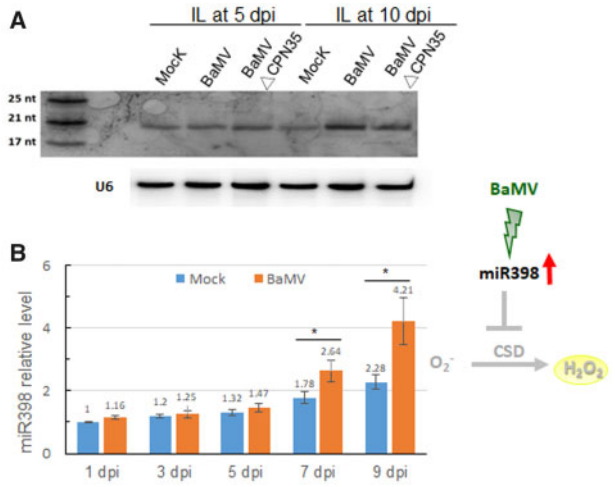


**Figure 6** Nb-miR398 was induced by BaMV and BaMV△CPN35 infection. Quantification of Nb-miR398 in mock- and BaMV-infected *N. benthamiana* by (A) RNA blot of ILs at 5 and 10 dpi and (B) RT-qPCR of ILs at 2-d intervals. Results from three plants per treatment per experiment were used for student's *t* test by three independent experiments. *$P < 0.05$.

*Agrobacterium* harboring a miR398-overexpression vector (pCVA-miR398) and an infectious clone of BaMV, pKB (Liou et al., 2014). Coinfiltrated leaves were harvested at 5 dpa for RNA purification followed by cDNA synthesis. RT-qPCR revealed that, relative to vector control samples, miR398b-3p levels were increased 60-fold (Supplemental Figure S5A) and BaMV levels were increased 1.84-fold (Figure 7A) in the miR398b-3p-overexpressing *N. benthamiana* leaves. Consequently, coincident with the high level of NbmiR398b-3p, RNA levels of the NbmiR398b-3p target genes, *NbCSD1 and NbCSD2*, were decreased in solely pCVA-miR398-infiltrated leaves. However, coinfiltration of pKB with pCVA-miR398 greatly increased *NbCSD1 and NbCSD2* gene expression despite NbmiR398b hyperaccumulation (Supplemental Figure S5B). Indeed, NbmiR398b-3p, NbCSD1, and NbCSD2 levels were increased to 2.77-, 3.52-, or 1.76-fold in BaMV-infected *N. benthamiana* compared to those in vector control-infected leaves, respectively, based on the data from three independent experiments (Supplemental Figure S5, A and B). Moreover, consistent with our results shown in Figure 2B, BaMV infection not only increased accumulation of NbmiR398b-3p but also of the RNAs of its target genes, *NbCSD1 and NbCSD2*. Thus, NbmiR398b-3p overexpression can enhance BaMV accumulation in *N. benthamiana*.

We further used short tandem target mimic (STTM) to block miR398 function (Supplemental Figure S6) and analyzed its effect on BaMV levels. *N. benthamiana* leaves were coinfiltrated with *Agrobacterium* harboring control pBin61 or pBin-miR398-STTM and *Agrobacterium* carrying pKB, and then subjected to RNA purification and RT-qPCR analysis at 5 dpa. In miR398-STTM and BaMV co-expressing leaves, BaMV levels were reduced to 0.37-fold relative to that in vector control plus BaMV coexpressing leaves (Figure 7B). Furthermore, in CSD2-silenced plants, BaMV levels had increased 22-fold relative to those in control (phytoene

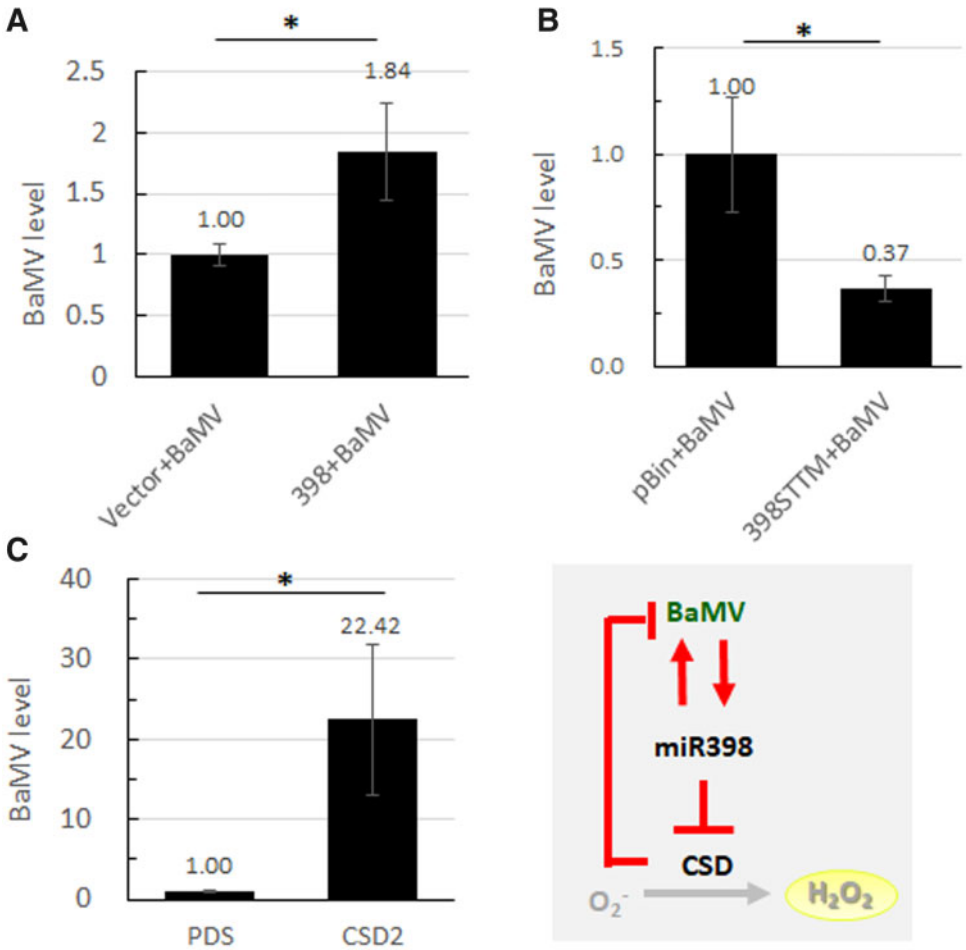


**Figure 7** BaMV level was regulated positively by miR398 and negatively by CSD2. Quantification of BaMV by RT-qPCR in (A) miR398 transiently overexpressed plants at 5 dpa, (B) miR398 STTM overexpressed plants at 2 dpa, and (C) CSD2 silenced plants at 7 dpa. Results from three independent experiments, three plants per treatment per experiment, were used for student's *t* test. $^*P < 0.05$.

desaturase [PDS]-silenced) plants (Figure 7C). Taken together, these analyses show that BaMV levels are regulated positively by miR398 and negatively by CSD2.

### NbCSD2 localization affects its regulation role on BaMV level

We have already shown that BaMV infection causes the failure of CSD2-GFP targeting to chloroplasts (Figure 3B) and CSD2 plays a negatively regulatory role on BaMV level (Figure 6B). We wondered whether CSD_noTP which resides in cytosol has any effects on BaMV accumulation. Therefore, we coinfiltrated *N. benthamiana* with *Agrobacteria* harboring a CSD2-HA or CSD2_noTP-HA overexpressed vector and pKB. Coinfiltrated leaves were harvested at 2 dpa for protein purification. By western blot, BaMV CP level was decreased 50% and increased 2.5-fold relative to vector control sample in CSD2-HA and CSD2_noTP-HA overexpressing *N. benthamiana* leaves, respectively, from three independent experiments (Figure 8). This result indicates that BaMV level was regulated negatively by chloroplastic CSD2 and positively by cytosolic CSD2_noTP.

## Discussion

Pathogen infection often triggers elevated levels of ROS such as superoxides and $H_2O_2$, resulting in a hypersensitive response (Lamb and Dixon, 1997). Elevated ROS levels enhance SA content and that of systemic acquired resistance marker proteins such as PATHOGENESIS RELATED 1/2 (Uknes et al., 1992; Maleck and Dietrich, 1999). *Plum plux virus* has been shown to induce chlorotic spots and increased ROS levels in pea plants (Diaz-Vivancos et al., 2008). Moreover, the levels of $H_2O_2$, superoxide, and *Cucumber mosaic virus* (CMV)-CP were intercorrelated with symptom development in CMV-infected *N. glutinosa*. (Lei et al., 2016; Jing Shang et al., 2018). Similarly, $H_2O_2$ was detected in *N. glutinosa and N. tabacum* cv. *Xanthi* infected with the incompatible *Tobacco mosaic virus* (TMV) or *Tomato mosaic tobamovirus* (Madhusudhan et al., 2009). In this study, we show that $H_2O_2$ accumulated in BaMV-induced

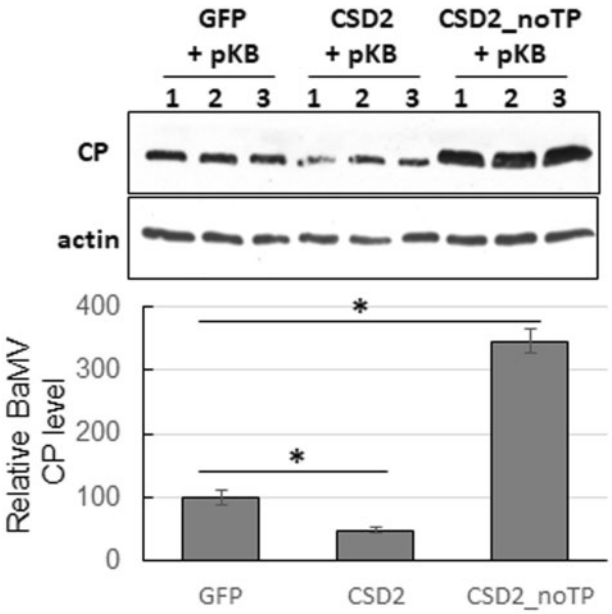


**Figure 8** Effects of different forms of CSD2 on BaMV accumulation. A, BaMV CP level of BaMV-infected leaves of GFP-, CSD2-HA-, or CSD2_noTP-HA-overexpressed *N. benthamiana* by protein blot at 2 dpa. B, Results from three independent experiments, three plants per treatment per experiment, were quantified by student's *t* test. $^*P < 0.05$.

symptomatic tissues of *N. benthamiana and B. distachyon*. However, $H_2O_2$ was undetectable by 3,3′-diaminobenzidine (DAB) staining of asymptomatic BaMV△CPN35-infected leaves (Figure 1, B and C). Furthermore, $H_2O_2$ treatment enhanced BaMV-induced chlorotic symptoms (Figure 4), but would not cause chlorosis in mock-infected leaves. This may be due to the sprayed $H_2O_2$ was not efficient and stable enough for chlorotic induction but it would be a priming signal to induce plant defense response upon pathogen infection. Moreover, levels of catalase that catalyzes $H_2O_2$ remained unchanged in BaMV- and BaMV△CPN35-infected leaves relative to mock-treated leaves (Supplemental Figure S7). In addition, chlorotic-like symptoms were induced in catalase-silenced *N. benthamiana* (Supplemental Figure S8). These results reveal a positive association between $H_2O_2$ and BaMV-induced symptoms, but it is independent of levels of BaMV CP.

SODs are one group of antioxidant enzymes responsible for ROS clearance (Gill and Tuteja, 2010). Our study shows that infection with BaMV or BaMV△CPN35 elevated both RNA and protein levels of NbCSD1 and NbCSD2 (Figure 2, A and B), but this effect was more pronounced for symptomatic BaMV-infected leaves than for asymptomatic BaMV△CPN35-infected leaves despite similar levels of BaMV CP and TGBp1 (Figure 2, A and B). Notably, $H_2O_2$ and prNbCSD2 solely accumulated in symptomatic BaMV-infected leaves but not in asymptomatic BaMV△CPN35-infected leaves (Figures 1, B and 2, B). These data demonstrate that increased $H_2O_2$ and antioxidant CSD levels are not associated with BaMV titer, but are linked to BaMV-induced symptoms. In addition, BaMV- but not BaMV△CPN35 triggered localization of most NbCSD2 in the cytosol (Figure 3). This outcome is likely due to impaired cleavage of the transit peptide of prNbCSD2, so that NbCSD2 could not be properly transported into chloroplasts, resulting in $H_2O_2$ accumulation and chlorotic symptoms upon BaMV infection. However, it has previously been shown that, in the case of CMV, the CP of the CMV-M, but not CMV-Q strain, can interact with chloroplastic ferredoxin I (Fd I) protein in the cytosol to disrupt chloroplast transportation of Fd I, thereby causing leaf chlorosis (Qiu et al., 2018).

CSDs are targets of the conserved miR398 in Arabidopsis (Sunkar and Zhu, 2004) and rice (Dugas and Bartel, 2008; Lu, 2010). By means of 5′-RLM-RACE and in vivo assay, we clearly show that miR398-3p regulates the *NbCSD1 and NbCSD2* genes via transcriptional cleavage in *N. benthamiana* (Figure 5). miR398-3p and its conserved targets, CSD1 and CSD2, regulate responses to biotic and abiotic stresses, as well as nutrient homeostasis, in many plant species (ZHu et al., 2011). Based on sRNA sequencing data, NbmiR398b-5p is more abundant than NbmiR398b-3p, with this latter being considered the functional miRNA (Yin et al., 2015). However, we showed that NbmiR398b-3p level and BaMV titer increased with infection progression in BaMV-infected *N. benthamiana* by northern blot (Figure 6). Thus, BaMV infection enhances levels of functional NbmiR398b-3p that targets NbCSDs. In addition, BaMV level is positively regulated by miR398 but negatively regulated by CSD2 (Figures 7, A–C and 8). Similar cases have been reported for fungal infection, with transiently overexpressed miR398b from common bean enhancing *Sclerotinia sclerotiorum* fungal lesioning of *N. benthamiana* (Naya et al., 2014). Therefore, different pathogens can manipulate miR398 levels to create a better environment for their infection. However, induced miR398 in BNYVV-infected *N. benthamiana* was able to activate immune system to restrict BNYVV infection through silencing a putative miR398 target gene, umecyanin, which is also involved in redox reactions (Liu et al., 2020). In our study, BaMV infection induced miR398 and its target CSD2 accumulation and localization of CSD2 in cytosol. Moreover, BaMV level was increased by overexpressed cytosolic CSD2_noTP-HA but reduced by chloroplastic CSD2-HA protein compared to that of GFP (Figure 8). In addition, BaMV level was also increased in CSD2-silenced plant. Therefore, we hypothesize that BaMV disrupts CSD2 chloroplast targeting to prevent defense signaling system.

We observed increased *NbCSD1 and NbCSD2* transcript levels despite hyperaccumulation of miR398 in BaMV-infected *N. benthamiana* leaves (Figure 2), as also found for BaMV-infected miR398-overexpressing *N. benthamiana* (Supplemental Figure S5). These results indicate that BaMV may induce transcription of *NbmiR398b-3p*, *NbCSD1*, and

*NbCSD2* simultaneously. Several virus-infected plants have been shown to exhibit miR398 accumulation, such as TMV- or *Oilseed rape mosaic tobamovirus*-infected *A. thaliana* (Bazzini et al., 2011; Hu et al., 2011), and *Potato virus X* (PVX)-, *Potato virus Y* (PVY)-, or *Tomato yellow leaf curl China virus* (TolCNV)-infected *N. benthamiana* (Naqvi et al., 2010; Pacheco et al., 2012). However, PVX and PVY infection resulted in higher *NbCSD* transcript levels, whereas ToLCNV infection reduced them (Naqvi et al., 2010; Pacheco et al., 2012). Whether or not virus-induced CSD transcript levels are altered may depend on different host-virus combinations.

In uninfected cells, ROS scavengers, CSDs, are tightly regulated by miR398. BaMV infection triggers upregulation of both miR398 and its target CSDs, which miR398 in turn positively regulates the BaMV titer. However, unlike the CSD2 resided in the chloroplasts of uninfected cells, BaMV induced abundant accumulation of PrNbCSD2 retained in the cytosol, leading to $H_2O_2$ hyperaccumulation and chlorotic symptoms (Figure 9). In addition, BaMV titer is greatly enhanced by overexpressed cytosolic NbCSD2 but reduced by chloroplastic NbCSD2 (Figure 8). Therefore, we uncover a mediator for BaMV-induced symptom formation and also a regulator of BaMV accumulation.

## Materials and methods

### Plant growth and BaMV inoculation

WT *N. benthamiana* and *B. distachyon* plants were grown in a growth chamber with 16-h/8-h light/dark cycles at 25°C. For each set of experiments, four 3-week-old *N. benthamiana* plants at the four-leaf stage were used, and three leaves of each plant were inoculated with virions. For *B. distachyon*, 7-d-old plants were inoculated with virions. Methods for inoculation were as described previously (Lin and Hsu, 1994; Lin et al., 1996; Liou et al., 2014), except that inocula contained 1 μg BaMV-S or BaMV△CPN35 virions (Lan et al., 2010).

### Histochemical staining of superoxide and hydrogen peroxide

Mock-, BaMV-, and BaMV△CPN35-ILs of *N. benthamiana* at 10 dpi or of *B. distachyon* at 7 dpi were detached for histochemical staining as described previously with minor modification (Fryer et al., 2003). Briefly, 0.2% (w/v) Nitrotetrazolium blue chloride (NBT) (Sigma-Aldrich) in 50 mM sodium phosphate buffer (pH 7.5) and 0.2% (w/v) DAB (Sigma-Aldrich) (pH 3.8) were used for superoxide and $H_2O_2$ detection. The detached leaves were immediately immersed in freshly prepared NBT or DAB staining buffer followed by vacuum infiltration for 10 min, before being kept in the dark overnight. Then, the leaves were washed once with distilled water and repeatedly shaken in 95% (v/v) alcohol for 20 min until the green color of chlorophyll had disappeared.

### Constructs

For the NbCSD2 localization assay, CSD2 cDNA was amplified with NbCSD2_XbaI-F and NbCSD2_BamHI-R, and then ligated into XbaI- and BamHI-treated pEpyon-32K (Chen et al., 2011) to generate pEpyon-CSD2-GFP. To construct

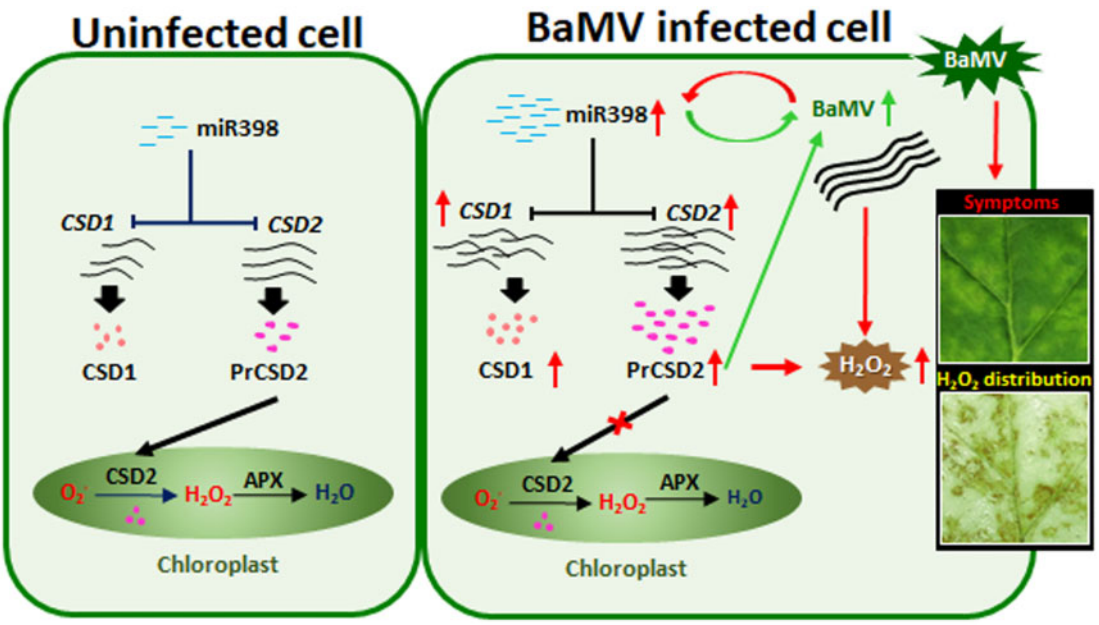


**Figure 9** Model of positive regulation of CSDs and $H_2O_2$ with BaMV-induced symptoms. In uninfected cell, *CSD1 and CSD2* levels are tightly regulated by miR398 and translated into CSD1 and PrCSD2 in cytosol, respectively. PrCSD2 is transported into chloroplasts as CSD2 whose transit peptide is cleaved. In chloroplasts, CSD2 catalyzes the conversion of superoxide ($O^{2-}$) into $H_2O_2$ which is catalyzed into water by ascorbate peroxidase (APX). After BaMV infection, miR398 and its target *CSD1 and CSD2* levels were induced. Moreover, BaMV infection induced PrCSD2 cytosolic retention which may result in $H_2O_2$ accumulation and lead to BaMV-induced chlorotic symptoms. Also, miR398 and prCSD2 can enhance BaMV accumulation.

pEpyon-CSD2_noTP-GFP in which NbCSD2 residues K59 and R60 were mutated to A, we used overlap PCR to generate a CSD2_noTP fragment by means of NbCSD2_*Xba*I-F, NbCSD2-noTP_R, NbCSD2-noTP_F, and NbCSD2_BamHI-R primers (all primers are detailed in Supplemental Table S1). Full cDNAs of BaMV and BaMV△CPN35 were cut from pBS2-8 and pBS△CPN35 (Lan et al., 2010) using XbaI and SacI, and then ligated into pEpyon-32K treated with XbaI and SacI enzymes to generate the pEpyon-BaMV and pEpyon- BaMV△CPN35 constructs, respectively. To prepare recombinant CSD1 and CSD2, we amplified the CDS of NbCSD1 and NbCSD2 and inserted them into pET15b before transforming them into *Escherichia coli* BL21. For protein production, we added 0.1 mM IPTG to *E. coli* culture at 28°C for 6 h before subjecting it to sonication. Recombinant CSD1 and CSD2 were then purified using His-tag/Ni-NTA resin.

For miR398 overexpression, we used a *CaLCuV*-based miRNA-expressing vector (Tang et al., 2010). The forward primer ath-pmiR398-F with a XbaI site and the reverse primer ath-pmiR398-R with a KpnI site were designed to amplify the miR398 precursor from *A. thaliana*, which was then ligated into XbaI/KpnI-treated *CaLCuV* T-DNA pCVA vector. To knock down miR398 expression, we used pCass (Ding et al., 1995) as the template to perform inverted PCR with the primer sets STTM F_*Swa*I/STTM R_*Swa*I and 398-STTM F_*Swa*I/398-STTM R_*Swa*I, respectively. The PCR product was cleaved by *Swa*I and self-ligated to generate pCass-STTM and pCass-398-STTM. Then, we used the plasmids pCass-STTM and pCass-398-STTM as templates to amplify the fragment containing the promoter, STTM sequence and terminator with the primers STTM_F_KpnI and STTM_R_SpeI, followed by digestion with KpnI and SpeI. The cleaved product was ligated into pBIN61 to generate the clones pBIN61-STTM and pBIN61-miR398-STTM. For CSD2-HA and CSD2_noTP-HA overexpression, pBin-NbCSD2-cDNA, and pEpyon-CSD2_noTP-GFP were used as template and using the specific primer set NbCSD2_*Xba*I-F and NbCSD2_HA_BamHI-R for amplification. The PCR product was cleaved with XbaI and BamHI before being subjected to PCR clean-up. Vector pEpyon-32K (Chen et al., 2011) was cleaved with XbaI and BamHI, followed by gel purification, and then ligated with the XbaI-NbCSD2_HA_*BamHI* fragment to generate pEpyon-NbCSD2_HA and pEpyon-NbCSD2_noTP-HA, respectively.

For CSD2 silencing, we amplified the NbCSD2 partial sequence from pBin-NbCSD2-cDNA with the specific primer set NbCSD2_KD_EcoRI and NbCSD2_KD_XhoI. The PCR product was treated with EcoRI and XhoI, subjected to PCR clean-up, and then cloned into pTRV2 (Ratcliff et al., 2001) that had been cleaved with EcoRI and XhoI, thereby generating pTRV2-CSD2. The NbCSD1 and NbCSD2 cDNAs were cloned into pGEMT-easy vector (Promega, Madison, WI, USA) by using the specific primers listed in Supplemental Table S1 and sequenced. The At-miR398b precursor was cloned into pBin61 vector with primers harboring KpnI or XbaI cutting sites. The pBin-miR398 and pBin-NbCSD1-cDNA or pBin-NbCSD2-cDNA constructs were transformed into *A. tumefaciens* C58C1 using the freeze-and-thaw method (Weigel and Glazebrook, 2006).

## *Agrobacterium* infiltration

All expression vectors were individually introduced into *A. tumefaciens* C58C1. For NbCSD2 localization, *A. tumefaciens* harboring pEpyon-CSD2-GFP, pEpyon-CSD2_noTP-GFP, pEpyon-BaMV, or pEpyon-BaMV△CPN35 were cultured overnight and induced with 100 μM acetosyringone in 10 mM $MgCl_2$ to a final optical density at 600 nm ($OD_{600}$) = 0.2. *Agrobacterium* containing pEpyon-CSD2-GFP was mixed with that containing pEpyon-BaMV or pEpyon-BaMV△CPN35 in a 1:1 ratio and infiltrated into *N. benthamiana* leaves, respectively.

For miR398 target site determination, we mixed *A. tumefaciens* cultures ($OD_{600}$ = 1) containing pBin-miR398 and pBin-NbCSD1-cDNA or pBin-NbCSD2-cDNA in a 1:1 ratio as indicated, and co-infiltrated them by syringe onto three leaves each of *N. benthamiana*. At 5 dpa, infiltrated leaves were harvested for RLM-RACE analysis. For the miR398 overexpression assay, *A. tumefaciens* cultures ($OD_{600}$ = 0.5) containing pCVA-miR398, pCVB, and pBin61 or pKB (Liou et al., 2014) were mixed in a 1:1:1 ratio and co-infiltrated onto *N. benthamiana*. At 5 dpa, infiltrated leaves were harvested for RT-qPCR analysis.

For miR398-knockdown assay, *A. tumefaciens* cultures ($OD_{600}$ = 0.5) containing pBIN-miR398-STTM or pBIN61 and pKB (Liou et al., 2014) were mixed in a 1:1 ratio and co-infiltrated into *N. benthamiana*. At 5 dpa, infiltrated leaves were harvested for RT-qPCR. For CSD2 silencing assay, *A. tumefaciens* cultures ($OD_{600}$ = 0.5) harboring pTRV1, pTRV2-PDS, or pTRV2-CSD2 were mixed in a 1:1 ratio and co-infiltrated onto the first, second, and third leaves of 18-d-old *N. benthamiana*. At 7 dpa, the fifth and sixth leaves were infiltrated with *A. tumefaciens* cultures ($OD_{600}$ = 0.5) containing pBin or pKB. The fifth and sixth leaves were harvested at 5 dpa for further analysis.

## Western blot analysis

Total protein was extracted (Vijaya Palani et al., 2006), separated by 12% sodium dodecyl sulfate–polyacrylamide gel electrophoresis, electrotransferred onto PVDF membranes (Immobilon-P; Millipore), and then detected with rabbit anti-CSD1, -CSD2, -BaMV-TGBp1 (Chang et al., 1997) , and -CP (Lin and Chen, 1991) antisera at 1:5,000 followed by probing with horseradish peroxidase-conjugated goat anti-rabbit antibody (Abomics, New Taipei City, Taiwan) at 1:10,000. NbCSD1- and NbCSD2-specific antisera were prepared by Abomics by immunizing rabbits with NbCSD1-specific synthetic polypeptides (N-DAPTTVTGNVSGLKPGFHG and N-GTAPFTITDKQVPLAGPQSI) conjugated to the C-terminal of carrier protein key-hole limpet hemocyanin (KLH) and NbCSD2-specific synthetic peptides (N-TTSTTNSLLFPVAAP

NTNPSPSLH-KLH and KLH-DGVAEATIIDNQIPLNGP NSV), respectively. A dilution of 1:5,000 was determined as optimal for western blot. Relative levels of actin were determined using mouse anti-actin (Sigma), which was used to normalize CSD1, CSD2, BaMV-TGBp1, and CP signals in the infected plants.

### RNA purification and northern-blot hybridization

Total RNA of harvested leaves was extracted using TriReagent (Invitrogen, Carlsbad, CA, USA) and loaded for northern-blot analysis. We adopted a previously described protocol for BaMV detection using a BaMV-specific L probe (Lin et al., 2010). For miR398 detection, an equal volume of 50% (v/v) deionized formamide with 1% (w/v) bromophenol blue was added to 10 μg total RNA following the procedure described for sRNA blotting (Lin et al., 2010), using a miR398 antisense probe (anti-miR398: 5′-CAGGGGCG ACCTGAGAACACA-3′) and anti-U6 probe (5′-AGGG GCCATGCTAATCTTCTC-3′).

### RT-qPCR analysis

Expression of BaMV and the putative miR398 target genes CSD1 and CSD2 was assayed by RT-qPCR. Two micrograms of total RNA was reverse-transcribed using a ToolsQuant II Fast RT Kit (Biotools, New Taipei City, Taiwan). The qPCR reactions were carried out in triplicate with SYBR-Green I Core Reagents (Life Technologies, Carlsbad, CA, USA) in a GeneAmp® 9700 Sequence Detection System (Life Technologies, Carlsbad, CA, USA) programmed to hold at 50°C for 2 min, then run at 95°C for 10 min, followed by 40 cycles of 95°C for 15 s and 60°C for 1 min. Specific primers for BaMV-RdRp, CSD1, CSD2, and actin (as internal control) are listed in Supplemental Table S2 for PCR reactions. PCR results reflected change in fluorescence signal of SYBR-Green I dye, and the Ct value for each reaction was determined in ABI Prism 7000 SDS software (Life Technologies, Carlsbad, CA, USA) setting the threshold of fluorescence as the exponential phase of amplifications.

### To determine miR398 target sites by RACE analysis

We employed a modified 5′-RLM-RACE PCR to determine the miR398 target sites of NbCSD1 and NbCSD2 by using a GeneRacer kit (Invitrogene). In general, total RNA was directly ligated to the RNA adaptor without pretreatment of calf intestinal phosphatase or tobacco acid pyrophosphatase and then reverse-transcribed using oligo dT primer. The transcribed cDNA was used for PCR and nested PCR with two sets of gene-specific primers and the adaptor-specific primer listed in Supplemental Table S2, respectively. The specific PCR product was gel-purified and cloned into pGEMT-easy vector for sequencing to determine the cleavage site of miR398.

### Confocal microscopy

Subcellular localization of NbCSD2 was observed on infiltrated leaves at 3 dpa. Images were obtained by means of laser scanning confocal microscopy (LSM 880 Meta; Carl Zeiss) using 488-nm laser excitation with 700 gains and 20% intensity and the emission spectrum was taken from 493 to 566 nm for GFP signal. Images of confocal microscopy were processed using the ZEN (Blue edition) program.

### $H_2O_2$ treatment

The 18-d-old *N. benthamiana* leaves were inoculated with mock-, BaMV-, or BaMV△CPN35 virions before or after spraying them with 5 mM $H_2O_2$ or water (as control) at 4-h intervals. ILs were harvested at 10 dpi for imaging and RT-qPCR analysis.

### Accession numbers

*NbCSD1*: Nbv5.1tr6233164, *NbCSD2*: Nbv5.1tr6229677, *AtCSD1*: At1g08830, *AtCSD2*: At2g28190.

## Supplemental Data

The following materials are available in the online version of this article.

**Supplemental Figure S1.** N-terminal 35 aa of BaMV CP were symptom determinants in *B. distachyon* and *N. benthamiana*.

**Supplemental Figure S2.** $H_2O_2$ accumulated in BaMV-induced chlorotic tissues of symptomatic leaves.

**Supplemental Figure S3.** Higher CSD activity in BaMV-infected leaves.

**Supplemental Figure S4.** Alignment of CSD1 and CSD2 from *Arabidopsis thaliana* and *N. benthamiana*.

**Supplemental Figure S5.** Expression of *miR398*, *NbCSD1 and NbCSD2* in miR398 overexpressed *N. benthamiana* leaves with or without BaMV infection harvested at 5 d post-agroinfiltration by RT-qPCR.

**Supplemental Figure S6.** Expression of *NbCSD2* in miR398-STTM overexpressed leaves of *N. benthamiana* harvested at 5 d post-agroinfiltration by RT-qPCR.

**Supplemental Figure S7.** Catalase level was not altered by BaMV and BaMV△CPN35 infection in *N. benthamiana*.

**Supplemental Figure S8.** Silencing of catalase induced chlorotic-like symptoms in *N. benthamiana*.

**Supplemental Table S1.** Primer lists for cloning.

**Supplemental Table S2.** Primer lists for RT-qPCR.

## Acknowledgments

We thank Dr Yule Liu for providing *CaLCuV*-based miRNA expression vector, Live-Cell-Imaging Core Laboratory and Genomic Technology Core Laboratory of the Institute of Plant and Microbial Biology, Academia Sinica, Taiwan for technical assistance.

## Funding

This work is supported by grants MOST NSC 101-2321-B-001-037, NSC-102-2321-B-001-026, and NSC 103-2321-B-001-013 from the Ministry of Science and Technology, Taiwan.

*Conflict of interest statement.* The authors declare that there is no conflict of interest.

## References


**Allan AC, Lapidot M, Culver JN, Fluhr R** (2001) An Early Tobacco Mosaic Virus-Induced Oxidative Burst in Tobacco Indicates Extracellular Perception of the Virus Coat Protein. Plant Physiol **126**: 97–108

**Asada K** (2006) Production and scavenging of reactive oxygen species in chloroplasts and their functions. Plant Physiol **141**: 391–396

**Abreu PMV, Gaspar CG, Buss DS, Ventura JA, Ferreira PCG, Fernandes PMB** (2014) Carica papaya MicroRNAs Are Responsive to Papaya meleira virus Infection. Plos One **9**: e103401

**Beauclair L, Yu A, Bouché N** (2010) microRNA-directed cleavage and translational repression of the copper chaperone for superoxide dismutase mRNA in Arabidopsis. Plant J **62**: 454–462

**Brousse C, Liu Q, Beauclair L, Deremetz A, Axtell MJ, Bouché N** (2014) A non-canonical plant microRNA target site. Nucleic Acids Res **42**: 5270–5279

**Bazzini AA, Manacorda CA, Tohge T, Conti G, Rodriguez MC, Nunes-Nesi A, Villanueva S, Fernie AR, Carrari F, Asurmendi S** (2011) Metabolic and miRNA profiling of TMV infected plants reveals biphasic temporal changes. PLoS One **6**: e28466

**Cao M, Du P, Wang X, Yu Y-Q, Qiu Y-H, Li W, Gal-On A, Zhou C, Li Y, Ding S-W** (2014) Virus infection triggers widespread silencing of host genes by a distinct class of endogenous siRNAs in Arabidopsis. Proc Natl Aca Sci U S A **111**: 14613–14618

**Chang BY, Lin NS, Liou DY, Chen JP, Liou GG, Hsu YH** (1997) Subcellular localization of the 28 kDa protein of the triple-gene-block of bamboo mosaic potexvirus. J Gen Virol **78**: 1175–9

**Chen M-K, Hsu W-H, Lee P-F, Thiruvengadam M, Chen H-I, Yang C-H** (2011) The MADS box gene, FOREVER YOUNG FLOWER, acts as a repressor controlling floral organ senescence and abscission in Arabidopsis. Plant J **68**: 168–185

**Clarke SF, Guy PL, Burritt DJ, Jameson PE** (2002) Changes in the activities of antioxidant enzymes in response to virus infection and hormone treatment. Physiol Plant **114**: 157–164

**Desikan R, Hancock JT, Coffey MJ, Neill SJ (1996)** Generation of active oxygen in elicited cells of Arabidopsis thaliana is mediated by a NADPH oxidase-like enzyme. FEBS Letters **382**: 213–217

**Díaz-Vivancos P, Clemente-Moreno MJ, Rubio M, Olmos E, García JA, Martínez-Gómez P, Hernández JA** (2008) Alteration in the chloroplastic metabolism leads to ROS accumulation in pea plants in response to plum pox virus. J Exp Bot. **59**: 2147–160

**DiMaio F, Chen C-C, Yu X, Frenz B, Hsu Y-H, Lin N-S, Egelman EH** (2015) The molecular basis for flexibility in the flexible filamentous plant viruses. Nat Struct Mol Biol **22**: 642–644

**Ding SW, Rathjen JP, Li WX, Swanson R, Healy H, Symons RH** (1995) Efficient infection from cDNA clones of cucumber mosaic cucumovirus RNAs in a new plasmid vector. J Gen Virol **76**: 459–464

**Dugas DV, Bartel B** (2008) Sucrose induction of Arabidopsis miR398 represses two Cu/Zn superoxide dismutases. Plant Mol Biol **67**: 403–417

**Fryer MJ, Ball L, Oxborough K, Karpinski S, Mullineaux PM, Baker NR** (2003) Control of Ascorbate Peroxidase 2 expression by hydrogen peroxide and leaf water status during excess light stress reveals a functional organisation of Arabidopsis leaves. Plant J **33**: 691–705

**Gill SS, Tuteja N** (2010) Reactive oxygen species and antioxidant machinery in abiotic stress tolerance in crop plants. Plant Physiol Biochem **48**: 909–930

**Hakmaoui A, Pérez-Bueno ML, García-Fontana B, Camejo D, Jiménez A, Sevilla F, Barón M** (2012) Analysis of the antioxidant response of Nicotiana benthamiana to infection with two strains of Pepper mild mottle virus. J Exp Bot **63**: 5487–5496

**Hakmaoui A, Perez-Bueno ML, Garcia-Fontana B, Camejo D, Jimenez A, Sevilla F, Baron M** (2012) Analysis of the antioxidant response of *Nicotiana benthamiana* to infection with two strains of Pepper mild mottle virus. J Exp Bot **63**: 5487–5496

**He XF, Fang YY, Feng L, Guo HS** (2008) Characterization of conserved and novel microRNAs and their targets, including a TuMV-induced TIR-NBS-LRR class R gene-derived novel miRNA in Brassica. FEBS Lett **582**: 2445–2452

**Hu Q, Hollunder J, Niehl A, Kørner CJ, Gereige D, Windels D, Arnold A, Kuiper M, Vazquez F, Pooggin M, et al. (2011)** Specific impact of tobamovirus infection on the Arabidopsis small RNA profile. PloS one **6**: e19549

**Hu Q, Hollunder J, Niehl A, Korner CJ, Gereige D, Windels D, Arnold A, Kuiper M, Vazquez F, Pooggin M, et al.** (2011) Specific impact of tobamovirus infection on the Arabidopsis small RNA profile. PLoS One **6**: e19549

**Huang YL, Han YT, Chang YT, Hsu YH, Meng M** (2004) Critical residues for GTP methylation and formation of the covalent m7GMP-enzyme intermediate in the capping enzyme domain of *Bamboo mosaic virus*. J Virol **78**: 1271–1280

**Huseynova IM, Sultanova NF, Aliyev JA** (2014) Histochemical visualization of ROS and antioxidant response to viral infections of vegetable crops grown in Azerbaijan. Plant Physiol Biochem **81**: 26–35

**Jagadeeswaran G, Saini A, Sunkar R** (2009) Biotic and abiotic stress down-regulate miR398 expression in Arabidopsis. Planta **229**: 1009–1014

**Jia X, Wang WX, Ren L, Chen QJ, Mendu V, Willcut B, Dinkins R, Tang X, Tang G** (2009) Differential and dynamic regulation of miR398 in response to ABA and salt stress in *Populus tremula* and *Arabidopsis thaliana*. Plant Mol Biol **71**: 51–59

**Jopling CL, Yi M, Lancaster AM, Lemon SM, Sarnow P** (2005) Modulation of hepatitis C virus RNA abundance by a liver-specific microRNA. Science **309**: 1577–1581

**Lamb C, Dixon RA** (1997) The oxidative burst in plant disease resistance. Annu Rev Plant Physiol Plant Mol Biol **48**: 251–275

**Lan P, Yeh WB, Tsai CW, Lin NS** (2010) A unique glycine-rich motif at the N-terminal region of *Bamboo mosaic virus* coat protein is required for symptom expression. Mol Plant Microbe Interact **23**: 903–914

**Lee CC, Ho YN, Hu RH, Yen YT, Wang ZC, Lee YC, Hsu YH, Meng M** (2011) The interaction between *Bamboo mosaic virus* replication protein and coat protein is critical for virus movement in plant hosts. J Virol **85**: 12022–12031

**Lei R, Du Z, Qiu Y, Zhu S** (2016) The detection of hydrogen peroxide involved in plant virus infection by fluorescence spectroscopy. Luminescence **31**: 1158–1165

**Lewsey M, Robertson FC, Canto T, Palukaitis P, Carr JP** (2007) Selective targeting of miRNA-regulated plant development by a viral counter-silencing protein. Plant J **50**: 240–252

**Li Y, Zhang QQ, Zhang JG, Wu L, Qi Y, Zhou J-M** (2010) Identification of microRNAs involved in pathogen-associated molecular pattern-triggered plant innate immunity. Plant Physiol **152**: 2222–2231

**Li F, Pignatta D, Bendix C, Brunkard JO, Cohn MM, Tung J, Sun H, Kumar P, Baker B** (2012) MicroRNA regulation of plant innate immune receptors. Proc Natl Acad Sci U S A **109**: 1790–1795

**Li Y, Zhang Q, Zhang J, Wu L, Qi Y, Zhou JM** (2010) Identification of microRNAs involved in pathogen-associated molecular pattern-triggered plant innate immunity. Plant Physiol **152**: 2222–2231

**Li YI, Cheng YM, Huang YL, Tsai CH, Hsu YH, Meng M** (1998) Identification and characterization of the *Escherichia coli*-expressed RNA-dependent RNA polymerase of *Bamboo mosaic virus*. J Virol **72**: 10093–10099

**Li YI, Shih TW, Hsu YH, Han YT, Huang YL, Meng M** (2001) The helicase-like domain of plant potexvirus replicase participates in formation of RNA 5′ cap structure by exhibiting RNA 5′-triphosphatase activity. J Virol **75**: 12114–12120

**Liang G, He H, Yu D** (2012) Identification of nitrogen starvation-responsive microRNAs in *Arabidopsis thaliana*. PLoS One **7**: e48951

**Lin N-S** (1991) Association of Bamboo Mosaic Virus (BoMV) and BoMV-Specific Electron-Dense Crystalline Bodies with Chloroplasts. Phytopathology **81**: 1551

**Lin KY, Cheng CP, Chang BC, Wang WC, Huang YW, Lee YS, Huang HD, Hsu YH, Lin NS** (2010) Global analyses of small interfering RNAs derived from *Bamboo mosaic virus* and its associated satellite RNAs in different plants. PLoS One **5**: e11928

**Lin MK, Chang BY, Liao JT, Lin NS, Hsu YH** (2004) Arg-16 and Arg-21 in the N-terminal region of the triple-gene-block protein 1 of *Bamboo mosaic virus* are essential for virus movement. J Gen Virol **85**: 251–259

**Lin MK, Hu CC, Lin NS, Chang BY, Hsu YH** (2006) Movement of potexviruses requires species-specific interactions among the cognate triple gene block proteins, as revealed by a trans-complementation assay based on the *Bamboo mosaic virus* satellite RNA-mediated expression system. J Gen Virol **87**: 1357–1367

**Lin N, Lin FZ, Huang TY, Hsu YH** (1992) Genome properties of *Bamboo mosaic virus*. Phytopathology **82**: 731–734

**Lin NS, Chen CC** (1991) Association of *Bamboo mosaic virus* (BoMV) and BoMV specific electron-dense crystalline bodies with chloroplasts. Phytopathology **81**: 1551–1555

**Lin NS, Hsu YH** (1994) A satellite RNA associated with bamboo mosaic potexvirus. Virology **202**: 707–714

**Lin NS, Lee YS, Lin BY, Lee CW, Hsu YH** (1996) The open reading frame of bamboo mosaic potexvirus satellite RNA is not essential for its replication and can be replaced with a bacterial gene. Proc Natl Acad Sci U S A **93**: 3138–3142

**Lin NS, Lin BY, Lo NW, Hu CC, Chow TY, Hsu YH** (1994) Nucleotide sequence of the genomic RNA of bamboo mosaic potexvirus. J Gen Virol **75** (Pt 9): 2513–2518

**Liou MR, Huang YW, Hu CC, Lin NS, Hsu YH** (2014) A dual gene-silencing vector system for monocot and dicot plants. Plant Biotechnol J **12**: 330–343

**Liu J, Fan H, Wang Y, Han C, Wang X, Yu J, Li D, Zhang Y** (2020) Genome-wide microRNA profiling using oligonucleotide microarray reveals regulatory networks of microRNAs in *Nicotiana benthamiana* during beet necrotic yellow vein virus infection. Viruses **12**: 310.

**Lu Y, Feng Z, Bian L, XieH, Liang J** (2010) miR398 regulation in rice of the responses to abiotic and biotic stresses depends on CSD1 and CSD2 expression. Funct Plant Biol **38**: 44–53

**Madhusudhan KN, Srikanta BM, Shylaja MD, Prakash HS, Shetty HS** (2009) Changes in antioxidant enzymes, hydrogen peroxide, salicylic acid and oxidative stress in compatible and incompatible host-tobamovirus interaction. J Plant Interact **4**: 157–166

**Maleck K, Dietrich RA** (1999) Defense on multiple fronts: how do plants cope with diverse enemies? Trends Plant Sci **4**: 215–219

**Mengistu AA, Tenkegna TA** (2021) The role of miRNA in plant-virus interaction: a review. Mol Biol Rep **48**: 2853–2861

**Nakasugi K, Crowhurst RN, Bally J, Wood CC, Hellens RP, Waterhouse PM** (2013) De novo transcriptome sequence assembly and analysis of RNA silencing genes of *Nicotiana benthamiana*. PLoS One **8**: e59534

**Naqvi AR, Haq QM, Mukherjee SK** (2010) MicroRNA profiling of tomato leaf curl New Delhi virus (tolcndv) infected tomato leaves indicates that deregulation of mir159/319 and mir172 might be linked with leaf curl disease. Virol J **7**: 281

**Naya L, Paul S, Valdes-Lopez O, Mendoza-Soto AB, Nova-Franco B, Sosa-Valencia G, Reyes JL, Hernandez G** (2014) Regulation of copper homeostasis and biotic interactions by microRNA 398b in common bean. PLoS One **9**: e84416

**Otsuka M, Jing Q, Georgel P, New L, Chen J, Mols J, Kang YJ Jiang Z, Du X, Cook R, et al.** (2007) Hypersusceptibility to vesicular stomatitis virus infection in Dicer1-deficient mice is due to impaired miR24 and miR93 expression. Immunity **27**: 123–134

**Otsuka M, Jing Q, Georgel P, New L, Chen J, Mols J, Kang YJ, Jiang Z, Du X, Cook R, et al.** (2007) Hypersusceptibility to vesicular stomatitis virus infection in Dicer1-deficient mice is due to impaired miR24 and miR93 expression. Immunity **27**: 123–134

**Pacheco R, Garcia-Marcos A, Barajas D, Martianez J, Tenllado F** (2012) PVX-potyvirus synergistic infections differentially alter microRNA accumulation in *Nicotiana benthamiana*. Virus Res **165**: 231–235

**Pilon M, Ravet K, Tapken W** (2011) The biogenesis and physiological function of chloroplast superoxide dismutases. Biochim Biophys Acta **1807**: 989–998

**Qiu Y, Zhang Y, Wang C, Lei R, Wu Y, Li X, Zhu S** (2018) *Cucumber mosaic virus* coat protein induces the development of chlorotic symptoms through interacting with the chloroplast ferredoxin I protein. Sci Rep **8**: 1205

**Ratcliff F, Martin-Hernandez AM, Baulcombe DC** (2001) Technical advance. Tobacco rattle virus as a vector for analysis of gene function by silencing. Plant J **25**: 237–245

**Reis RS, Eamens AL, Waterhouse PM** (2015) Missing pieces in the puzzle of plant microRNAs. Trends Plant Sci **20**: 721–728

**Riedle-Bauer M** (2000) Role of reactive oxygen species and antioxidant enzymes in systemic virus infections of plants. J Phytopathol **148**: 297–302

**Rodriguez M, Munoz N, Lenardon S, Lascano R** (2012) The chlorotic symptom induced by Sunflower chlorotic mottle virus is associated with changes in redox-related gene expression and metabolites. Plant Sci **196**: 107–116

**Satish D, Mukherjee SK, Gupta D** (2019) PAmiRDB: a web resource for plant miRNAs targeting viruses. Sci Rep **9**: 4627

**Schott G, Mari-Ordonez A, Himber C, Alioua A, Voinnet O, Dunoyer P** (2012) Differential effects of viral silencing suppressors on siRNA and miRNA loading support the existence of two distinct cellular pools of ARGONAUTE1. EMBO J **31**: 2553–2565

**Schult P, Roth H, Adams RL, Mas C, Imbert L, Orlik C, Ruggieri A, Pyle AM, Lohmann V** (2018) microRNA-122 amplifies hepatitis C virus translation by shaping the structure of the internal ribosomal entry site. Nat Commun **9**: 2613

**Serrano I, Audran C, Rivas S** (2016) Chloroplasts at work during plant innate immunity. J Exp Bot **67**: 3845–3854

**Shang J, Zhang L, Jia Q, Tang Z-Q, Yuan S, Yang H, Zhang M, Huang Y** (2018) Early ROS accumulation in chloroplasts of *Nicotiana glutinosa* infected by *Cucumber mosaic virus*. Int J Agric Biol **21**: 149–154

**Song XS, Wang YJ, Mao WH, Shi K, Zhou YH, Nogues S, Yu JQ** (2009) Effects of *Cucumber mosaic virus* infection on electron transport and antioxidant system in chloroplasts and mitochondria of cucumber and tomato leaves. Physiol Plant **135**: 246–257

**Sunkar R, Kapoor A, Zhu J-K** (2006) Posttranscriptional induction of two Cu/Zn superoxide dismutase genes in Arabidopsis is mediated by downregulation of miR398 and important for oxidative stress tolerance. Plant Cell **18**: 2051–2065

**Sunkar R, Kapoor A, Zhu JK** (2006) Posttranscriptional induction of two Cu/Zn superoxide dismutase genes in Arabidopsis is mediated by downregulation of miR398 and important for oxidative stress tolerance. Plant Cell **18**: 2051–2065

**Sunkar R, Li YF, Jagadeeswaran G** (2012) Functions of microRNAs in plant stress responses. Trends Plant Sci **17**: 196–203

**Sunkar R, Zhu JK** (2004) Novel and stress-regulated microRNAs and other small RNAs from Arabidopsis. Plant Cell **16**: 2001–2019

**Suzuki T, Ikeda S, Kasai A, Taneda A, Fujibayashi M, Sugawara K, Okuta M, Maeda H, Sano T** (2019) RNAi-mediated down-regulation of dicer-like 2 and 4 changes the response of 'moneymaker' tomato to potato spindle tuber viroid infection from tolerance to lethal systemic necrosis, accompanied by up-regulation of miR398, 398a-3p and production of excessive amount of reactive oxygen species. Viruses **11**: 344

**Tagami Y, Inaba N, Kutsuna N, Kurihara Y, Watanabe Y** (2007) Specific enrichment of miRNAs in *Arabidopsis thaliana* infected with tobacco mosaic virus. DNA Res **14**: 227–233

**Tang Y, Wang F, Zhao J, Xie K, Hong Y, Liu Y** (2010) Virus-based microRNA expression for gene functional analysis in plants. Plant Physiol **153**: 632–641

**Trobaugh DW, Gardner CL, Sun C, Haddow AD, Wang E, Chapnik E, Mildner A, Weaver SC, Ryman KD, Klimstra WB** (2014) RNA viruses can hijack vertebrate microRNAs to suppress innate immunity. Nature **506**: 245–248

**Trobaugh DW, Sun C, Bhalla N, Gardner CL, Dunn MD, Klimstra WB** (2019) Cooperativity between the 3′ untranslated region microRNA binding sites is critical for the virulence of eastern equine encephalitis virus. PLoS Pathog **15**: e1007867

**Uknes S, Mauch-Mani B, Moyer M, Potter S, Williams S, Dincher S, Chandler D, Slusarenko A, Ward E, Ryals J** (1992) Acquired resistance in Arabidopsis. Plant Cell **4**: 645–656

**Varallyay E, Valoczi A, Agyi A, Burgyan J, Havelda Z** (2010) Plant virus-mediated induction of miR168 is associated with repression of ARGONAUTE1 accumulation. EMBO J **29**: 3507–3519

**Vijaya Palani P, Kasiviswanathan V, Chen JC, Chen W, Hsu YH, Lin NS** (2006) The arginine-rich motif of *Bamboo mosaic virus* satellite RNA-encoded P20 mediates self-interaction, intracellular targeting, and cell-to-cell movement. Mol Plant Microbe Interact **19**: 758–767

**Wang J, Mei J, Ren G** (2019) Plant microRNAs: biogenesis, homeostasis, and degradation. Front Plant Sci **10**: 360

**Weigel D, Glazebrook J** (2006) In planta transformation of Arabidopsis. CSH Protocols **2006**

**Wu TH, Liao MH, Kuo WY, Huang CH, Hsieh HL, Jinn TL** (2011) Characterization of copper/zinc and manganese superoxide dismutase in green bamboo (*Bambusa oldhamii*): cloning, expression and regulation. Plant Physiol Biochem **49**: 195–200

**Wung CH, Hsu YH, Liou DY, Huang WC, Lin NS, Chang BY** (1999) Identification of the RNA-binding sites of the triple gene block protein 1 of bamboo mosaic potexvirus. J Gen Virol **80** (Pt 5): 1119–1126

**Yamasaki H, Abdel-Ghany SE, Cohu CM, Kobayashi Y, Shikanai T, Pilon M** (2007) Regulation of copper homeostasis by micro-RNA in Arabidopsis. J Biol Chem **282**: 16369–16378

**Yamasaki H, Abdel-Ghany SE, Cohu CM, Kobayashi Y, Shikanai T, Pilon M** (2007) Regulation of copper homeostasis by micro-RNA in Arabidopsis. J Biol Chem **282**: 16369–16378

**Yamasaki H, Hayashi M, Fukazawa M, Kobayashi Y, Shikanai T** (2009) SQUAMOSA promoter binding protein-like7 Is a central regulator for copper homeostasis in Arabidopsis. Plant Cell **21**: 347–361

**Yang CC, Liu JS, Lin CP, Lin NS** (1997) Nucleotide sequence and phylogenetic analysis of a bamboo mosaic potevirus isolate from common bamboo (*Bambusa vulgaris* McClure). Bot Bull Acad Sin **38**: 77–84

**Yin K, Tang Y, Zhao J** (2015) Genome-wide characterization of miRNAs involved in N gene-mediated immunity in response to tobacco mosaic virus in *Nicotiana benthamiana*. Evol Bioinform Online **11**: 1–11

**Zhang C, Wu Z, Li Y, Wu J** (2015) Biogenesis, function, and applications of virus-derived small RNAs in plants. Front Microbiol **6**: 1237

**Zhu C, Ding Y, Liu H** (2011) MiR398 and plant stress responses. Physiol Plant **143**: 1–9